This paper describes objective technical results and analysis. Any subjective views or opinions that might be expressed in the paper do not necessarily represent the views of the U.S. Department of Energy or the United States Government.

SAND2019-10727J

The Oklahoma Geological Survey Statewide Seismic Network

Jacob I. Walter[1]*, Paul Ogwari[1], Andrew Thiel[1], Fernando Ferrer[1], Isaac Woelfel[1], Jefferson C. Chang[2], Amberlee P. Darold[3], Austin A. Holland[4],

[1]Oklahoma Geological Survey, University of Oklahoma, 100 E. Boyd St., Norman, OK 73019, USA

[2]U.S. Geological Survey, Hawaiian Volcano Observatory, 51 Crater Rim Dr., Hawai‘i National Park, Hawaii, HI 96718, USA

[3]U.S. Geological Survey, Cascades Volcano Observatory, 1300 SE Cardinal Court Bldg. 10, Vancouver, WA 98683, USA

[4]Sandia National Laboratories, 1515 Eubank Blvd SE, Albuquerque, NM 87123, USA

*Correspondence to: jwalter@ou.edu

Sandia National Laboratories is a multimission laboratory managed and operated by National Technology & Engineering Solutions of Sandia, LLC, a wholly owned subsidiary of Honeywell International Inc., for the U.S. Department of Energy’s National Nuclear Security Administration under contract DE-NA0003525.

Abstract

The Oklahoma Geological Survey (OGS) monitors seismicity throughout the state of Oklahoma utilizing permanent and temporary seismometers installed by OGS and other agencies, while producing a real-time earthquake catalog. The OGS seismic network was recently added to the Advanced National Seismic System (ANSS) as a self-supporting regional seismic network (RSN) and earthquake locations and magnitudes are automatically reported through USGS and are part of the ANSS Comprehensive Earthquake Catalog. In Oklahoma, prior to 2009, background seismicity rates were about 2 M3.0+ earthquakes per year, which increased to 579 and 903 M3.0+ earthquakes in 2014 and 2015, respectively. The peak in the seismicity rate has since fallen to 624, 304, and 194 M3.0+ earthquakes in 2016, 2017, and 2018, respectively. The catalog is complete down to M2.2 from mid-2014 to present, despite the significant workload for a primarily state-funded regional network. That astonishing uptick in seismicity has been largely attributed to wastewater injection practices. The OGS provides the Oklahoma Corporation Commission (OCC), the agency responsible for regulating oil and gas activities within the state, with technical guidance and earthquake products that inform their "traffic-light" mitigation protocol and other mitigating actions. We have initiated a citizen-scientist driven, educational seismometer program by installing Raspberry Shake geophones throughout the state at local schools, museums, libraries, and state parks. The seismic hazard of the state portends a continued need for expansion and densification of seismic monitoring throughout Oklahoma.

1. Background

1.1. Geology and historical earthquakes

The underlying geology of Oklahoma can be characterized by marine sedimentation with brief periods of uplift and subsidence. The long period of subsidence created deep sedimentary units that contribute to Oklahoma being a vast resource of hydrocarbon source rocks and deposits (Lawson and Luza, 1995). Those periods of subsidence were terminated by protracted periods of uplift, which brought granite to the surface in southern Oklahoma and formed the tectonic zone known as the Amarillo-Wichita uplift. That tectonic feature, which includes uplifted granite, extends west-northwest from south-central Oklahoma into the Texas Panhandle, and forms a belt of seismicity active in the present (Walter et al., 2018). In central and northern Oklahoma, the subsurface geology consists of fractured intrusives and crystalline basement (Shah and Keller, 2017) overlain by the sediments from the aforementioned periods of subsidence and marine sedimentation.

Oklahoma is riddled with structural features comprised of steeply dipping north-south fault systems that separate geologic provinces (e.g. Northcutt and Campbell, 1995). The structural features include zones that act as traps for hydrocarbons and thus, considerable effort has gone into mapping the geology in these areas. The Nemaha fault system, one such north-south feature, that crosses central Oklahoma formed from a tectonic event in the Mississippian and consists of uplifted blocks 5-8 km wide bounded by faults on either side (Lawson and Luza, 1995). East of the Nemaha uplift there are a series of several grabens separated by (from west to east) the Wilzetta, Keokuk, Wewoka, Weleetka, and East Mountain fault zones (Dycus, 2013; Dudek, 2014). These named faults, while easily identified through well log analysis, include subtle surface expressions of small antithetical faults along the main trace.

In southern Oklahoma, the Meers Fault is a large fault that is plausibly capable of rupturing in a M7.0+ earthquake. The most recent evidence of rupture has been dated to as recently as ~1,300 years ago (Crone and Luza, 1990). The fault is one of two faults in North America, east of the Rocky Mountains, with visible surface offset that displaces Holocene sediments and thus possibly represents the largest known earthquake hazard in the Central United States. Over the last few decades, OGS scientists and other collaborating institutions have engaged in paleoseismological and shallow geophysical surveys to ascertain the seismic sequence history. Trenching and surface mapping suggests that the rupture length would be consistent with at least a M7.0+ event (Luza et al., 1987). Preliminary probabilistic seismic hazard analysis (PSHA) from the Meers Fault suggests that such an earthquake might cause widespread damage, though additional studies on recurrence interval, rupture lengths, and other variables are needed if PSHA were conducted for building design guidance or other purposes (Baker and Holland, 2013).

Oklahoma has experienced at least 5 magnitude 5.0 or greater earthquakes within the written historical record. Of those earthquakes, 4 of the 5 M5.0+ earthquakes have occurred within the last 8 years. The large earthquake that occurred outside of the last 8 years was the M5.5 El Reno earthquake (Figure 1) that caused moderate damage in El Reno and Oklahoma City including toppled chimneys and smokestacks, cracked and loosened bricks on buildings, and broken windows and dishes, including a crack in the State Capitol that was approximately 15 meters long. Shaking was reported across Oklahoma, including in Kansas, Arkansas, Iowa, Kansas, Missouri, Nebraska, and Texas. It reportedly triggered a landslide in eastern Oklahoma (Regmi and Walter, 2019). Based on the presence of a few wastewater injection wells within the same county as the event and the nature of the macroseismic reported intensities from

93 newspapers and other archives, Hough and Page (2015) suggested that the El Reno earthquake
94 was possibly induced. They based this suggestion on the spatial proximity of wells and the
95 limited historical macroseismic observations seem to be consistent with similar observations
96 from more modern measurements of induced earthquakes. However, wastewater injection was
97 common across the state and the macroseismic signature of induced earthquakes results from the
98 shallowness of the source, as suggested by Hough and Page (2015). Depth is not a particularly
99 diagnostic criteria for determining causation since most Oklahoma earthquakes, both tectonic
100 and induced, are shallow relative to other tectonic zones.
101

Date	Name	Magnitude	County
September 3, 2016	Pawnee Earthquake	5.8	PAWNEE
November 6, 2011	Prague Earthquake	5.7	LINCOLN
April 9, 1952	El Reno Earthquake	5.5	CANADIAN
February 13, 2016	Fairview Earthquake	5.1	WOODS
November 7, 2016	Cushing Earthquake	5.0	PAYNE
October 22, 1882	Choctaw Nation Earthquake	4.8	SE Oklahoma
November 5, 2011	Prague foreshock	4.8	LINCOLN
January 7, 2016	Fairview foreshock	4.8	WOODS
November 8, 2011	Prague aftershock	4.8	LINCOLN
November 19, 2015	Alfalfa County Earthquake	4.7	ALFALFA

102 ***Table 1:*** *Significant Oklahoma earthquakes*

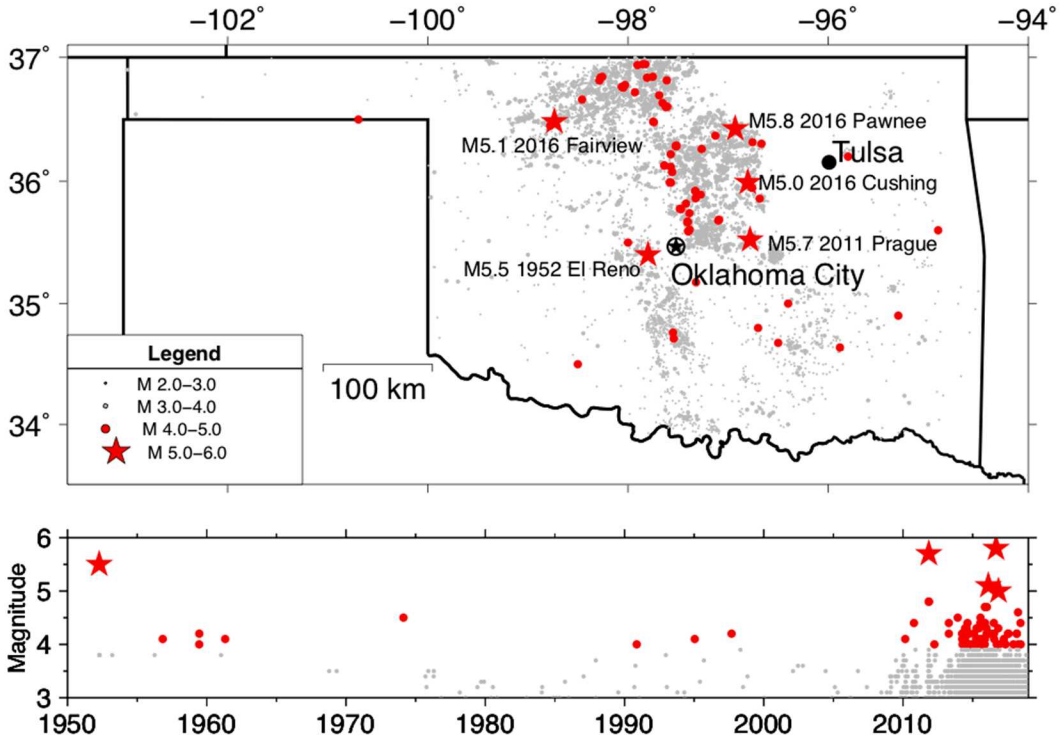

Figure 1: *Historical earthquakes in Oklahoma from the OGS catalog (https://ogsweb.ou.edu/eq_catalog) with symbols corresponding to earthquake magnitudes and labels for those earthquakes greater than or equal to M5.0. Note that seismicity from adjacent states is not mapped.*

1.2. Induced seismicity

Late in the evening at 10:53 PM local time on November 5, 2011, Oklahomans east of Oklahoma City were awakened by what was then the largest earthquake in recorded history. That earthquake, a M5.7 with an epicenter near Prague, was later eclipsed in size by the September 3, 2016 M5.8 earthquake near Pawnee, OK. The Prague earthquake, which actually occurred on

November 6, 2011 03:53 UTC, caused some injuries and damage was substantial, including famously collapsing a turret and damaging other turrets at St. Gregory's University in Shawnee, OK. The larger mainshock was preceded by a strong M 4.8 foreshock about 20 hours prior. The scientific community largely agrees that the Prague earthquake was probably induced by nearby wastewater injection (Keranen et al., 2013; Sumy et al., 2017). While increased seismicity in central Oklahoma was suspected as being induced by wastewater injection, this earthquake ushered in a wave of scientific studies that more solidly established the relationship.

Subsequent to the Prague earthquake, the seismicity rate continued drastically rising across various regions of Oklahoma (Figure 2) in what was later understood to be a rise concurrent with an increase in saltwater disposal (Walsh and Zoback, 2015; Weingarten et al. 2015). Several clusters of previously unmapped faults had significant seismic activity including areas that culminated in several large earthquakes including the November 2011 Mw 5.7 Prague earthquake (Holland et al., 2012; Keranen et al., 2013), the February 2016 Mw 5.1 Fairview earthquake (Yeck et al., 2016), the September 2016 Mw 5.8 Pawnee earthquake (Yeck et al., 2017; Walter et al., 2017; Chen et al., 2018), and the November 2016 Mw 5.0 Cushing earthquake.. The rate of earthquakes (M3.0+) across the United States mid-continent and especially in Oklahoma has dramatically increased since 2009 (Ellsworth, 2013). In Oklahoma prior to 2009, background seismicity rates were about 2 M 3.0+ earthquakes per year which increased to 579 and 903 M 3.0+ earthquakes in 2014 and 2015, respectively.

The increase in seismicity in Oklahoma was roughly coincident with the last oil and gas boom focused around the Mississippian Limestone and Hunton Limestones. Those formations contain substantial amounts of co-produced formation brines (Murray and Holland, 2014). The widespread use of horizontal production wells and hydrofracturing to make those wells

138 economical also led to extracting vast amounts of brine byproducts, which required subsequent
139 disposal. Common disposal practices involved disposing of wastewater in deep underground
140 injection wells completed into upper parts of the basement and the karst Arbuckle Group, which
141 directly overlies the basement. From 2010 to late 2014, statewide disposal rates increased from
142 ~30 million bbls/month to ~90 million bbls/month. The increase in seismicity rate roughly
143 corresponded to the increase in monthly injection rates, though with sometimes a lag greater than
144 a year or so in many sub-regions of Oklahoma (Langengruch and Zoback, 2016; Goebel et al.,
145 2017). That observation, coupled with the depth of the seismicity mostly occurring within
146 basement rocks and sometimes along previously-mapped basement faults led to the general
147 conclusion that wastewater disposal within the Arbuckle Group was inducing earthquakes across
148 Oklahoma (Walsh and Zoback, 2015).
149 Since peaks in wastewater injection and seismicity in late 2014 and late 2015,
150 respectively, wastewater injection and seismicity rates have fallen substantially to ~40 million
151 bbl/mo and less than 10 earthquakes M3.0+ per month. The decrease in injection, which
152 plausibly drives the decrease in seismicity, is in part due to state-mandated reductions in
153 allowable daily disposal rates (OCC, 2016a) and oilfield economics; the technical achievements
154 of hydrofracturing and horizontal wells that fueled the domestic mid-continent energy boom
155 contributed to a global oversupply and subsequent industry downturn as the price of oil collapsed
156 in 2014/2015 (Stocker et al., 2018).
157 Much of the activity in the last 8 years corresponds to a broad area in north-central
158 Oklahoma where most of the deep wastewater injection disposal occurs into the Arbuckle Group.
159 However, several large events have occurred across southern Oklahoma associated with the
160 aforementioned Amarillo-Wichita uplift in southwest Oklahoma (Walter et al., 2018) and

Ouachita thrust belt in southeast Oklahoma, including the M4.8 1882 Choctaw Nation earthquake (Hough and Page, 2015). The historical earthquake catalog includes small earthquakes (< M4.0) across mapped and unmapped fault structures in Oklahoma, including in areas without any hydrocarbon extraction or disposal activities. Thus, the tectonic seismicity rate across Oklahoma is possibly elevated relative to other regions in the Central United States. Since developing hydrocarbons from unconventional shale plays seems to lead to an increase in seismicity (e.g. Ellsworth, 2013), it is perhaps no surprise that industrial activities in the last decade exacerbated the underlying seismic hazard in Oklahoma.

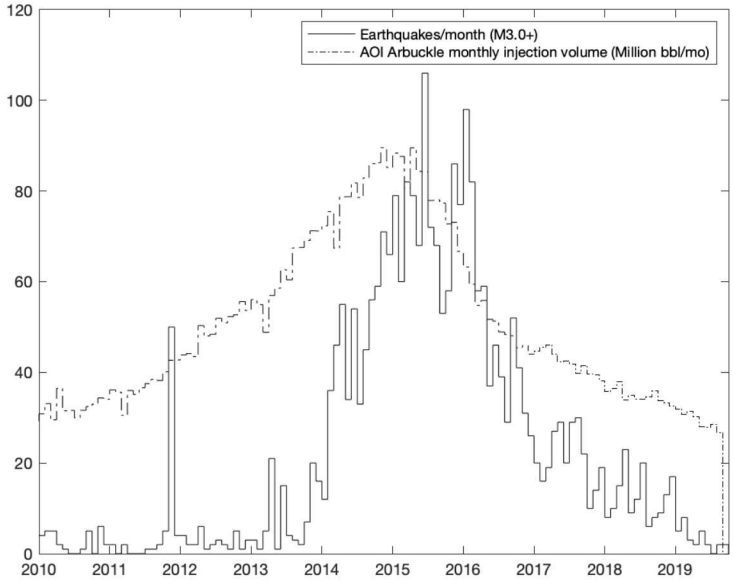

Figure 2: *Seismicity rate (earthquakes M3.0+ per month) from the OGS catalog in black and Arbuckle Group wastewater disposal monthly volumes within the OCC area of interest (AOI) that comprises much of north-central Oklahoma.*

2. Regional seismic network

2.1. Leonard facility and past regional studies

The Oklahoma Geological Survey has been in existence since 1908, having been included in the State's Constitution that was ratified in 1907. While some early earthquakes were recorded as having been felt by eyewitness reports, most earthquakes in the state were not instrumentally detected prior to the 1960s (Lawson and Luza, 1995). In 1961, the Jersey Production Research Company installed a seismograph in Leonard, Oklahoma about 40 km southeast of Tulsa. The seismograph and surrounding land were later donated to the University of Oklahoma and it was called the Leonard Geophysical Observatory, staffed and administered by the OGS. This seismograph had the station code TUL and borehole instrumentation now monitors ground motions on the same site adjacent to the surface site with station code TUL3 operated by the USGS as part of the N4 network. When installed, TUL was a long-period sensor and not particularly suited to recording local earthquakes for regional monitoring purposes. In 1973, a short-period seismograph was also installed at TUL, though the ability to detect local earthquakes relied on felt reports with the instrumental record providing further location and magnitude constraints.

In the period between 1977-1993, OGS operated a statewide network with radio telemetry for stations near the Leonard facility. Those stations were later converted to digitally transmit their data or digitally record locally. From the period of about 1976-2010 there were about 8 permanent seismographs operating in the state. During this time period OGS scientists conducted a regional study on the feasibility for nuclear power facilities was funded by the Nuclear Regulatory Commission (Luza and Lawson, 1982) that identified microseismicity across the Nemaha fault zone. In addition, other local studies were supported by various agencies for identifying local earthquakes along specific features, such as near the Meers Fault (Luza et al., 1987), for example.

2.2. Transportable Array and early seismic network

In the period between 2009-2012, Transportable Array (TA) stations as part of the USArray initiative, funded by the National Science Foundation, were installed at ~70 km spacing throughout the state. Stations were intended to operate for a period of ~2 years and be utilized for structural seismology studies. Serendipitously for seismologists with interests in induced seismicity, the arrival of TA stations corresponded with the aforementioned rise in earthquake activity associated with the rise in unconventional oil and gas operations across the mid-continent, and later, in the Appalachian Basin of the eastern US (e.g. Brudzinski and Kozłowska, 2019). Since much of the NSF investment was incurred during construction of the sites, local agencies were given the opportunity to purchase or "adopt" some permanent stations. In 2011-2012, the OGS adopted and continues maintaining stations U32A, W35A, X34A, and X37A as part of the OK network. The OK network serves as the permanent station network code for the OGS RSN.

The adopted TA stations and stations operated by other agencies (e.g. WMOK) formed the core nucleus of the monitoring stations for the OGS network. In addition, some TA stations continued operating as the N4 network with maintenance handled by IRIS and funded by NSF before being transferred to USGS, including two stations in Oklahoma (T35B and the aforementioned TUL3). Around this time, as funds were made available, several additional stations were added over the next several years, including a subset of stations donated by a local energy company near the Oklahoma City metropolitan area. After large earthquakes, USGS also added several temporary stations across the state and those stations (network code GS) were incorporated into OGS monitoring. Shortly after the Fairview and Pawnee earthquakes and

related swarm activity, the Y9 and Y7 networks, respectively, consisting of temporary stations provided by IRIS/PASSCAL, were installed to capture aftershock activity as part of NSF-funded rapid response programs.

2.3. Current network

In anticipation of hydraulic fracturing across a new unconventional play called the SCOOP/STACK in a region to the west and southwest of Oklahoma City, OGS installed additional IRIS/PASSCAL stations (ZP) starting in early 2016. Later, we consolidated all the temporary networks under one network code (O2) in 2018 (Figure 3). All OK and O2 stations are streamed in real-time on a public seedlink buffer (rtserve.ou.edu port 18000) that the Incorporated Research Institutions for Seismology (IRIS) Data Management Center (DMC) utilizes for archival and USGS utilizes for detection purposes at the National Earthquake Information Center (NEIC). Metadata for these stations are available through IRIS. While the O2 and OK networks consist of stations the OGS manages directly, data from the AG, C0, GM, GS, N4, TX, and US networks are also accessed through the IRIS real-time seedlink buffer.

In addition to the professional grade seismometers used in these networks (i.e.: Streckeisen STS-2, Guralp CMG-6T, Guralp CMG-3T, etc.), Raspberry Shake 1D seismometers have been installed at various locations around the state. We purchased several of these one component sensors primarily for outreach and education. We have installed them in schools, libraries, museums, and state parks, along with accompanying monitors that show the real-time data and also daylong helicorder plot for the installed stations. Surrounding the monitors, we install explanatory placards describing seismograms, how to locate earthquakes, why wastewater injection induces earthquakes, etc. In addition to the educational role, they may serve to

supplement some of the detection capabilities for the primary seismic network (e.g. Anthony et al., 2018). Provisionally, we have tested using these streams for locating earthquakes when coverage by primary stations is lacking, for example, in eastern Oklahoma.

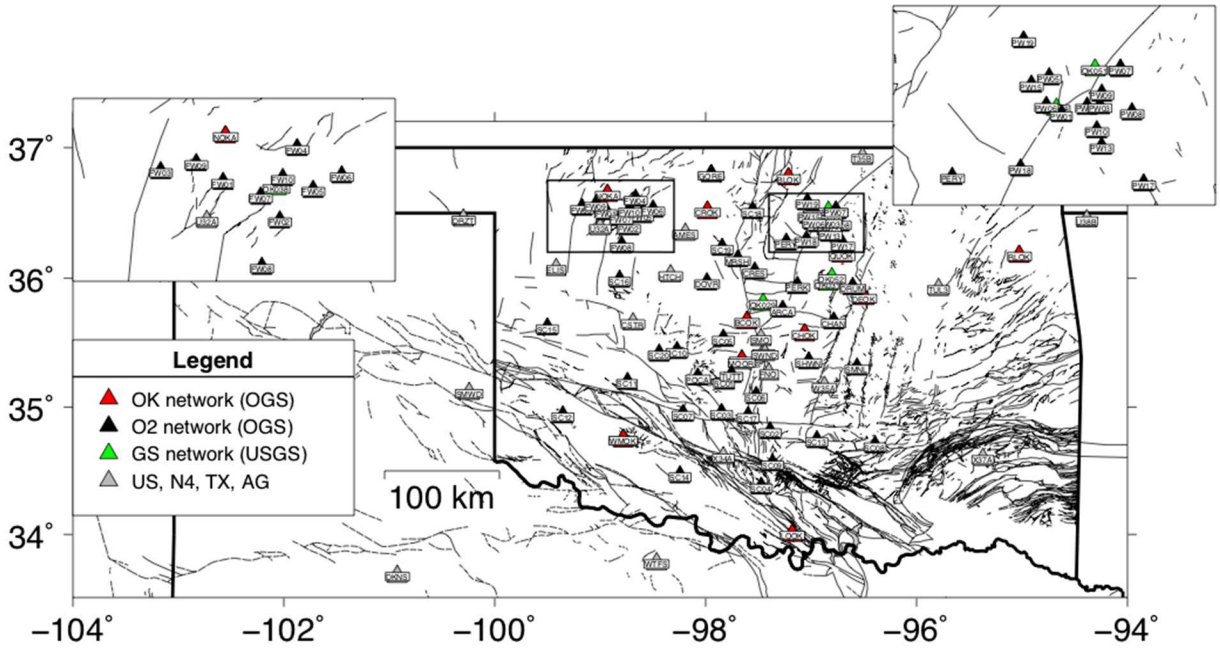

Figure 3: *Current OGS Statewide Network configuration, including stations operated by OGS (OK, O2) and stations operated by other agencies that are utilized in real-time earthquake analysis. Oklahoma faults are mapped from Marsh and Holland (2016).*

3. Earthquake monitoring

3.1. Real-time earthquake location and magnitude reporting

Prior to late 2018, automatic earthquake picking and association was performed using a python-based picker and associator largely built in-house (Chen and Holland, 2016). After events were identified, analysts would refine phase picks, pick polarities, and compute focal mechanisms through the SeisAn software (Havskov and Ottermöller, 1999). Once reviewed,

events would populate an OGS database and then be transmitted to USGS through their Product Distribution Layer (PDL). At the time, OGS had no official role within the ANSS and thus USGS analysts at NEIC that received EQXML files would sometimes include earthquake solutions derived from OGS or from NEIC. In other cases, the OGS event location would be used in conjunction with USGS moment tensor analysis for magnitude. Thus, the ANSS Comprehensive Catalog for Oklahoma downloaded at USGS (https://earthquake.usgs.gov/data/comcat/) versus OGS (https://ogsweb.ou.edu/eq_catalog/) may contain several inconsistencies and these should be noted for hazards analysis or research purposes (Figure 4). In late 2018, OGS joined ANSS as a self-funded network and there are tentative plans to resolve some of these historical incongruities between the earthquake catalogs.

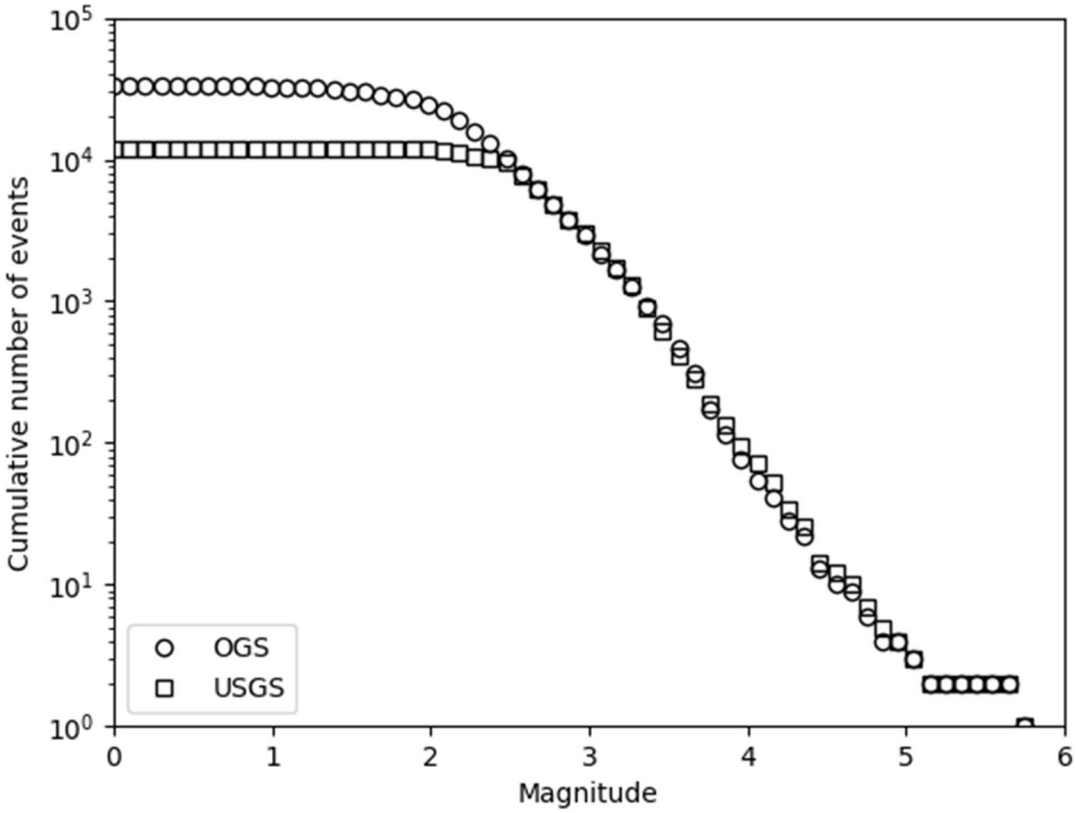

Figure 4: *Cumulative Gutenberg-Richter style plot of both the USGS (green) and OGS (red) earthquake catalogs.*

Current OGS earthquake monitoring consists of a SeisComP3 (SC3) system capable of detecting, locating, and computing an earthquake magnitude within seconds of an earthquake occurring (Weber et al., 2007). The preliminary localization and magnitude determination is completed even before body waves reach all stations within the state. As time progresses and further data is collected, the automatic locator system modifies the estimated magnitude, depth, and location with the acquisition of additional data. We distribute the SC3 workload across several virtual machines (VMs) within a private cloud managed at the University of Oklahoma (Figure 5). Data flow comes from network stations to an RTPD server and a server running acquisition modules connects to that RTPD server as well as outside seedlink connections to either IRIS or individual stations that utilize Q330 dataloggers. A separate VM connects to the SC3 acquisition VM and runs the public seedlink connection. The SC3 processing VM processes the waveform data and produces candidate automatic locations and magnitudes. Core components of SC3 are open source and we also utilize proprietary modules commercialized by gempa GmbH to improve the reliability of earthquake association.

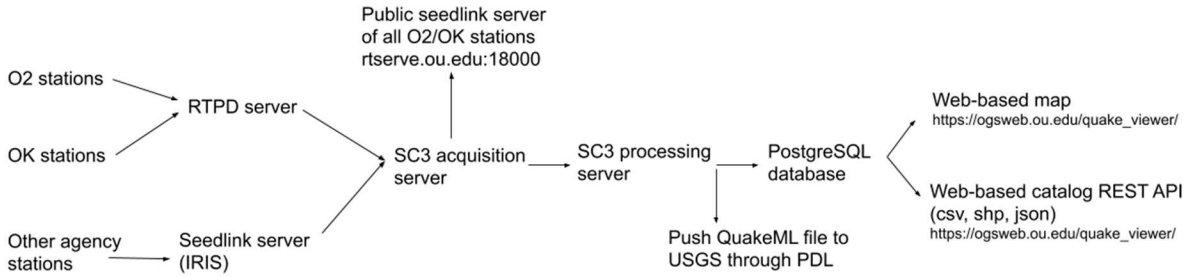

Figure 5: *Flow diagram of earthquake monitoring system.*

291 During regular business hours, manual processing of earthquakes in SC3 is streamlined
292 such that events can be processed within minutes. Due to the lack of resources to staff
293 earthquake monitoring at all hours, we have made several operational decisions related to public
294 publishing of automatic solutions. First, in order to provide timely earthquake information, we
295 initially post automatic earthquake solutions. We developed a python listener script that runs
296 continually within the SC3 processing VM and determines whether automatically-located events
297 should populate the public database that meet certain minimum criteria, such as phase count and
298 association quality. Once these criteria are met, an event is written to a separate PostgreSQL
299 database on a separate VM. Once written to the database, the public is able to view these events
300 by downloading the catalog (https://ogsweb.ou.edu/eq_catalog/) or viewing the OGS recent
301 earthquakes webpage (https://ogsweb.ou.edu/quake_viewer/), but are listed as *'preliminary.'*
302 Once an event is reviewed by an analyst, the event is updated within the PostgreSQL database
303 and the public designation changes to *'reviewed.'* In cases of larger events (M 3.8 or greater)
304 during off-business hours, the processing system is accessed remotely to verify and review
305 events.

306 Through our official inclusion in ANSS, earthquake locations and magnitudes pushed to
307 USGS through PDL and are authoritative within Oklahoma. For internal purposes, we still locate
308 and review events within approximately one county in surrounding states as shaking from these
309 earthquakes could plausibly be felt within the state and we are charged with providing that
310 timely information to Oklahoma citizens. These state-adjacent events are not forwarded through
311 PDL but available through OGS web applications.

312 While we have tuned our local magnitude (M_L) calculation so that estimates of local
313 magnitude should be equivalent to USGS moment magnitude (M_w) estimates, for larger events

we defer to the moment magnitude calculated at NEIC because they are using waveform-based approach to estimate M_w. It is widely accepted in the community that a waveform-based approach is preferred relative to a Richter-like approach that effectively averages several maximum-amplitude observations.

3.2. Local magnitude (M_L) calculation

For each horizontal component, we compute the one-half the peak-to-trough amplitude, *A*, on the WA simulated displacement (in mm) with 2080 sensitivity and damping constant of 0.7, rather than the manufacturer-reported sensitivity of 2800 and damping constant of 0.8 (Uhrhammer and Collins, 1990). Amplitudes are measured, automatically, within a 25 second window from the P-wave pick and the peak-to-trough amplitude is divided by a factor of 2. During regular business hours, during event review an analyst will manually select a window corresponding to the maximum and minimum values of the S arrival for each horizontal component. Amplitudes are measured for each horizontal component at a station and then averaged for the station magnitude estimate.

As is commonly done in regional networks we formulate an amplitude distance-correction so that magnitude may be determined at each station within the network where:

$$M_L = \square\square\square\square - \square\square\square A_0(\square)$$

where x is the distance (km) from the epicenter. The final event magnitude is median of all station magnitudes within 10-160 km epicentral distance. We choose a minimum of 10 km epicentral distance because at close epicentral distances, and within the WA synthetic passband, there may be source-radiated energy in the spectrum above the Nyquist frequency. Thus, the maximum trace amplitudes that are used to calculate the station M_L could be underestimated. We

choose 160 km as the maximum window because this corresponds to the epicentral distance at which the P_n head wave traveling along the uppermost mantle would arrive at a station before the direct P wave (See supplementary material). Local magnitude should be determined from direct body waves (Hutton and Boore, 1987) and so we do not consider more distant estimates of earthquake magnitude where the first P arrival would have traveled as a head wave along the crust-mantle interface.

We determined the fit to the previous equation by using amplitudes from local network stations for earthquakes with a corresponding USGS-determined W-phase moment magnitude (Mww) or regional moment tensor magnitude (Mwr). Since that magnitude is predetermined, we used the magnitude in the previous equation and come up with values for the -logA0 value, which should be common to earthquakes of all magnitudes. We fit an equation of the form a*log10(x)+b*x+c to the scatter of *-logA0* values and determine coefficients: a=2.01, b=-0.0057, and c=-0.45. Functionally, in SC3, the function is replaced by a table of values, where epicentral distances between points are interpolated between table entries. The function (green line) and interpolated table values (maroon line), as implemented in SC3, are shown in Figure 6. It should be noted that this logA0 function differs from one previously used at OGS up until late 2018 (Darold et al., 2014).

Within the WA synthetic response, earthquakes in the region produce surface waves with relatively larger amplitude than the S wave. When the peak amplitude is derived from a larger window that is larger than the first few seconds after S-arrival, then the subsequent magnitude is relatively higher than the magnitude based on analyst-selected body wave amplitudes. Hence, there can be a difference between automatic (USGS M_L and OGS-automatic) and analyst-derived M_L. We typically find this corresponds to an initial underestimation of event magnitude of ~0.1

to 0.2 magnitude units observed in both NEIC-reported M_L and automatic-M_L OGS reports. We analyzed 36 common events in 2019 for an area west of Oklahoma City and Norman and found that event magnitudes were 0.1 magnitude units lower than either the USGS M_L (0.1 median lower) or mbLg magnitudes (0.1 median lower). We note that the systematic difference between OGS and USGS M_L values stem from a difference between using analyst-selected windows around the S-wave (OGS) and automatic windows where the largest amplitude is used within the coda (USGS procedure for M_L).

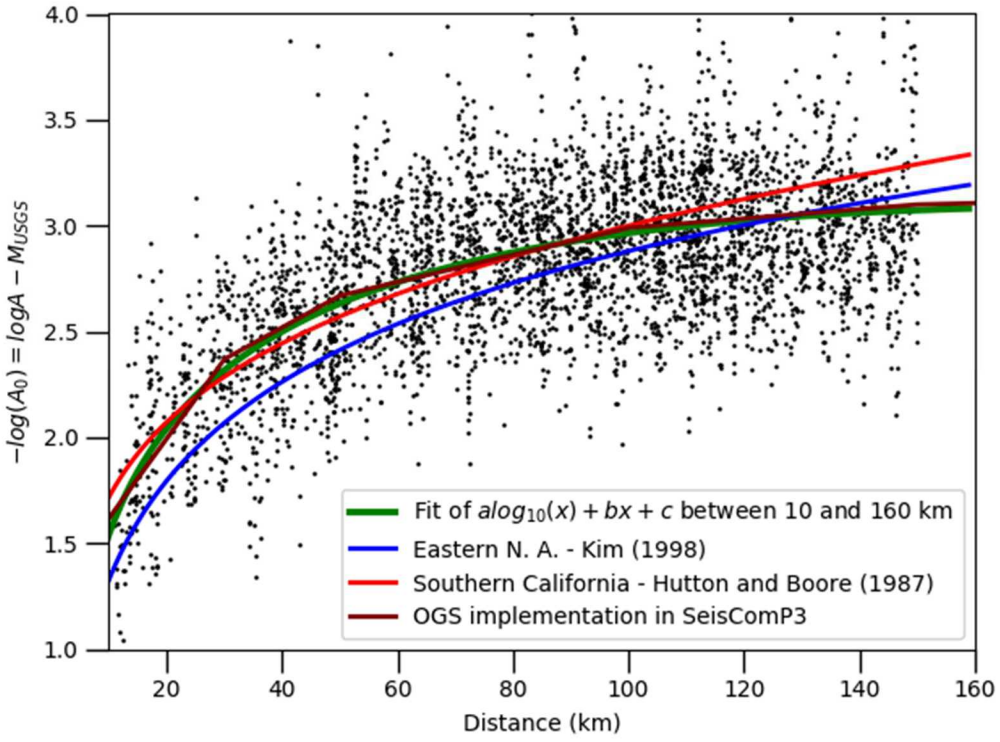

Figure 6: *logA0 values for earthquakes that included USGS-recorded magnitude was derived using a moment tensor solution (Mwr or Mww). The logA0 term derives from the Richter equation described in the text and is used for calculating local magnitudes for smaller earthquakes.*

4. Earthquake hazard and risk

The USGS updates the long-term National Seismic Hazard Map approximately every 6 years. With the aforementioned increase in seismicity associated with unconventional resource plays in the last decade, the USGS sought to identify the short-term hazard in areas across the central US and released short-term seismic hazard updates for 2016, 2017, and 2018 (Petersen et al., 2016; Petersen et al., 2017; Petersen et al., 2018). Those updates followed the same methodology as the long-term model (Petersen et al., 2014) including declustering earthquake catalogs so that the earthquake behavior approaches a Poissonian process whereby random, independent events (earthquakes) occur at a specific activity rate. Assuming the underlying rate of occurrence and the notion that there is a power-law distribution for occurrence of earthquake sizes (Gutenberg-Richter law), then one is able to estimate the underlying seismic hazard (Rosson et al., 2019).

For the short-term hazard updates, USGS utilized earthquake occurrences within a short time period (2 years with the most recent year weighted more heavily) to forecast the seismic hazard into the next year. In the most recent forecast for 2018, Petersen et al. (2018) forecasted a 10-14% chance of moderate damage for an area adjacent to the Oklahoma City metro area and encompassing a broad swath of north-central Oklahoma. This represents a hazard nearly equivalent some areas of California (Petersen et al., 2014). It is unclear whether USGS will not continue to update the short-term hazard model as a USGS spokesman is cited in a July 8, 2019 Tulsa World article (Associated Press, 2019): “The reason is because that induced seismicity has been decreasing every year since we did our first forecast back in 2015-2016, and as such, we're moving on to different priorities.”

The state of Oklahoma is home to approximately 4 million people. Metropolitan areas of Oklahoma City and Tulsa are most vulnerable to the earthquake risk due to the larger number of structures and built environment. Since the seismic risk to the built environment is associated with the degree of shaking experienced during an earthquake, the OGS has identified soils statewide that may be susceptible to stronger shaking relative to other areas (Pritchett et al., 2017). In that study, we categorized areas across the state according to NEHRP soil liquefaction classification scheme and found that both major metropolitan zones (Oklahoma City and Tulsa) may be more susceptible to stronger shaking and subsequent damage due to their proximity to the North Canadian and Arkansas Rivers, respectively. Further urban mapping would be required to better understand the soil structures that would be susceptible to strong shaking or liquefaction effects.

Most of the induced earthquakes have occurred on previously unmapped faults (Skoumal et al., 2019) highlighting the difficulty of predicting earthquake hazard from induced seismicity. Many of these faults do not have sufficient displacement to be detectable with active-source seismic imaging. In early 2015, the OCC issued a directive to limit wastewater injection to depths above the crystalline basement by “plugging-back” wells that extend into the basement. This was supposed to reduce the pore-pressure communication between the Arbuckle Group and the basement. However, many basement faults extend into the Arbuckle Group enabling pore-pressure migration into the basement. By mid-2015, the OCC put in a plan to reduce the daily injection rates and volumes in selected areas of interest (AOI) with increased seismicity rate. This was complemented by a downturn of oil prices which forced reduction of production in regions deemed uneconomical for production.

In early 2016, the OCC took further measures by implementing daily reporting of injection data into the Arbuckle Group, an improvement to the monthly summary reports that are filed annually (OCC, 2015). Timely reporting of the more refined data provides the opportunity to more effectively mitigate seismic hazard in a timely manner, especially in response to large earthquakes; on numerous occasions the OCC would rapidly shut-in (halt disposal operations) or modify permits for reduced disposal in wells near larger (M4.0+) events. A recent study suggests that some of these "rapid-response" actions were effective in reducing the rate of aftershocks following several large events, including the Pawnee and Cushing earthquakes (Goebel et al., 2019).

Starting December 2016, the OCC designated the SCOOP/STACK region as an AOI and proactively implemented a stoplight protocol (OCC, 2016b) to mitigate hydraulic fracturing triggered seismicity (Holland, 2013; Skoumal et al., 2018). This protocol relies on the timely OGS catalog of earthquake epicenters and magnitudes to quickly determine the prescribed mitigating measures. As the earthquakes within wastewater injection AOI have declined, hydraulic fracturing in the SCOOP/STACK region has contributed almost half of the seismicity in Oklahoma in 2019. Thus, effective management and mitigation of earthquake risk continues to be dependent upon effective monitoring by the OGS RSN.

5. Conclusions

As we outlined in prior sections, the OGS has been dedicated to understanding earthquake hazards for the last several decades. We summarized some of those more recent efforts and describe the current regional seismic network that is part of ANSS. Earthquakes occur along the myriad faults across the state, whether or not that fault slip was promoted by

wastewater injection. Starting around 2009, the rate of M3.0+ earthquakes rose from about 2 or 3 per year to 579 and 903 in 2014 and 2015, respectively. While that rate has since declined to pre-2014 rates, the seismic hazard in Oklahoma remains elevated relative to its tectonic background.

We have, in an ad-hoc fashion since 2010, built the infrastructure for a seismic network capable of robustly detecting seismicity, with near real-time seismic processing and dissemination of information to the public. Our research into induced seismicity has provided the Oklahoma Corporation Commission with the technical guidance to more safely and effectively mitigate earthquake hazards. Furthermore, our work includes significant outreach and education of the populace regarding earthquake hazards. All these past, present, and future efforts should reduce the seismic risk for loss of property and life. Because Oklahoma does not have a substantial history of earthquakes, much work remains.

6. Data and Resources

Waveform data recorded by OGS is available in real-time at the IRIS Data Management Center at ds.iris.edu under Federated Digital Seismic Network codes OK (OGS; doi.org/10.7914/SN/OK), O2 (OGS 2018+; doi.org/10.7914/SN/O2), Y7 (OGS/OU 2016-2019; doi.org/10.7914/SN/Y7_2016), Y9 (OGS/OU 2016-2019; doi.org/10.7914/SN/Y9_2016), ZP (OGS 2016-2019; doi.org/10.7914/SN/ZP_2016). The USGS M_L values and amplitudes used for comparison were accessed through the ANSS Comprehensive Catalog (https://earthquake.usgs.gov/data/comcat/, last accessed June 2019). The OGS earthquake map is updated in real-time (https://ogsweb.ou.edu/quake_viewer/) and the catalog can be downloaded for specific time periods and magnitude ranges (https://ogsweb.ou.edu/eq_catalog/). Some of the custom listener scripts and other utilities for the SC3 system that were developed by OGS are

463 available through public repositories (https://github.com/jakewalter/seiscomp_tools) or available
464 by contacting the authors.
465
466 **7. Acknowledgements**
467 The authors acknowledge funding from the State of Oklahoma through OGS core funding as
468 well as supplementary funding through the Oklahoma Secretary for Energy and the
469 Environment. We thank the analysts and other staff at OGS over the years that assisted in the
470 earthquake monitoring efforts. Finally, we thank Oklahoma landowners for allowing us access to
471 their properties to install seismographs.

472 Sandia National Laboratories is a multimission laboratory managed and operated by National Technology
473 and Engineering Solutions of Sandia, LLC, a wholly owned subsidiary of Honeywell International Inc.,
474 for the U.S. Department of Energy's National Nuclear Security Administration under contract DE-
475 NA0003525. This paper describes objective technical results and analysis. Any subjective views or
476 opinions that might be expressed in the paper do not necessarily represent the views of the U.S.
477 Department of Energy or the United States Government.
478
479
480
481 **Appendix**
482 **Cross-over distance at which Pn phase arrives first**
483 In Oklahoma, we analyzed the data to determine the crossing point at which the first
484 phase arrival is the Pn phase, which is the P-wave from an earthquake that travels as a head wave
485 along the crust-mantle boundary. We plot the P-wave travel times with a reduced velocity
486 corresponding to mantle P-wave velocity (8.3 km/s) and find the crossover distance at which the
487 first P-wave is not direct arrival but the head wave that travels along the upper mantle (Pn). We

estimate *h*, the thickness of the crust with the following equation (Mahani and Kao, 2018; Stein and Wysession, 2003):

$$\square_0 = \square / \left(2\sqrt{(1/\square_0^2 - 1/\square_1^2}\right)$$

where v_1 is the mantle velocity, v_0 is the reciprocal of the slope of in Figure A1, and τ is the y-intercept or the head wave travel-time at zero distance. Thus the critical distance, x_c, at which the P-wave arrival is the head wave can be calculated:

$$x_c = 2\,\square_0 \frac{\square_0/v_1}{\sqrt{1 - (\square_0^2/\square_1^2)}}$$

We use these calculations to guide our earthquake processing where we do not utilize magnitude measurements that are greater than 160 km from the earthquake because the crust is approximately 41 km thick, the distance at which Pn phases are the first P phase recorded is approximately 160 km.

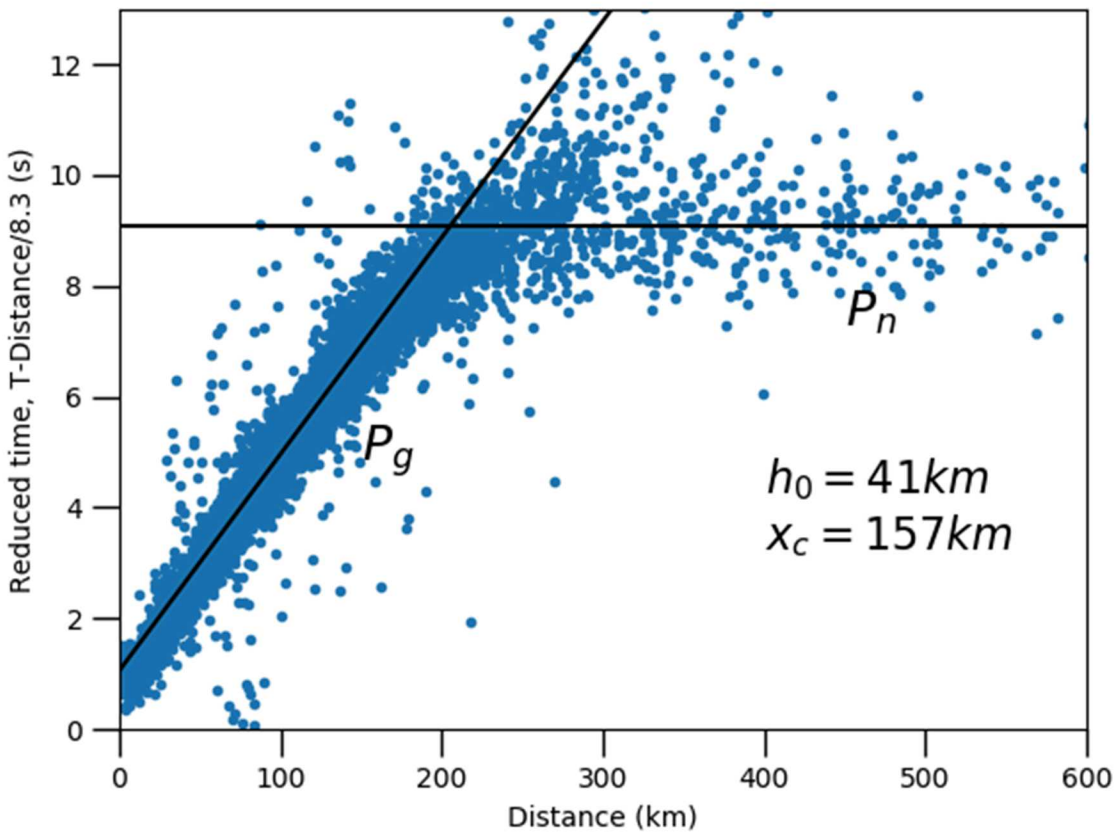

Figure A1: *Analyst-picked P-wave arrival time relative to event origin time.*

References

Anthony, R. E., A. T. Ringler, D. C. Wilson, and E. Wolin (2018). Do Low□Cost Seismographs Perform Well Enough for Your Network? An Overview of Laboratory Tests and Field Observations of the OSOP Raspberry Shake 4D, Seismological Research Letters, 90 (1): 219–228, doi: https://doi.org/10.1785/0220180251.

Associated Press (2019). Number of Oklahoma Earthquakes Drops for 4th Straight Year, Tulsa World, July 8, 2019, https://www.tulsaworld.com/number-of-oklahoma-earthquakes-drops-for-th-straight-year/article_e26eca2a-abce-59fe-90bf-9703297b5df8.html (Accessed August 2019).

Baker, E. M., and A. A. Holland (2013). Probabilistic Seismic Hazard Assessment of the Meers Fault, Southwestern Oklahoma: Modeling and Uncertainties, *OGS Special Publication* 2013-02.

Brudzinski, M. R. and M. Kozlowska (2019). Seismicity induced by hydraulic fracturing and wastewater disposal in the Appalachian Basin, USA: a review, *Acta Geophysica* 67 (1), 351-364.

Chen, C., and A. A. Holland (2016). PhasePApy: A Robust Pure Python Package for Automatic Identification of Seismic Phases, *Seismol. Res. Lett.*, 87(6), DOI: 10.1785/0220160019.

Chen, X., C. Pennington, J. Haffener, J. C. Chang, X. He, Z. Zhan, S. Ni, and J. I. Walter (2017). The Pawnee earthquake as a result of the interplay among injection, faults and foreshocks, *Scientific Reports*, 7: 4945, doi:10.1038/s41598-017-04992-z.

Crone, A. J., and Luza, K. V. (1990). Style and timing of Holocene surface faulting on the Meers fault, southwestern Oklahoma, *Geological Society of America Bulletin*, v. 102, p. 1-17.

Darold, A., A. A. Holland, C. Chen, and A. Youngblood (2014). Preliminary analysis of seismicity near Eagleton 1–29, Carter County, *OGS Open□File Report* OF2□2014.

Dudek, J. E. (2014), Understanding the geologic structure and kinematics of the Keokuk fault zone in east-central Oklahoma, *University of Tulsa MS thesis*.

Dycus, M. N. (2013), Structural characterization of the Wilzetta fault zone; Lincoln, Pottawatomie, and Creek Counties, Oklahoma, *University of Tulsa MS thesi*s.

Ellsworth, W. L. (2013). Injection-induced earthquakes, *Science* 341 (6142), 1225942

Goebel, T. H. W., J. I. Walter, K. Murray, and E. E. Brodsky (2017). Comment on "How will induced seismicity in Oklahoma respond to decreased saltwater injection rates?" by C. Langenbruch and M. D. Zoback, *Science Advances*, 3:8, doi:10.1126/sciadv.1700441.

Goebel, T., Z. Rosson, E. E. Brodsky, and J. I. Walter (2019). Aftershock deficiency of induced earthquake sequences during rapid mitigation efforts in Oklahoma, *Earth and Planet. Sci. Lett.*, 522, p. 135–143, doi: 10.1016/j.epsl.2019.06.036.

Havskov, J., and L. Ottemoller (1999). SeisAn Earthquake Analysis Software, *Seismol. Res. Lett.*, 70 (5): 532–534, doi: https://doi.org/10.1785/gssrl.70.5.532

Holland, A., K. Keranen, and E. Atekwana (2012). Preliminary Results of the November 5, 2011, Mw5.6 Earthquake Sequence Prague, Oklahoma, *Assoc. of Env. and Eng. Geol. AEG News*, 55(2), 15-16.

556 Holland, A. A. (2013). Earthquakes triggered by hydraulic fracturing in south-central Oklahoma,
557 *Bull. Seismol. Soc. Am.*, 103(3), 1784–1792, https://doi.org/10.1785/0120120109.
558
559 Hough, S. E., and M. Page (2015). A century of induced earthquakes in Oklahoma?, *Bull.*
560 *Seismol. Soc. Am.*,105(6), 2863–2870.
561
562 Hutton, L. K., and Boore, D. M. (1987). The ML Scale in Southern California, *Bull. Seismol.*
563 *Soc. Am.*, v. 77, no. 6, p. 2074-2094.
564
565 Keranen, K. M., H. M. Savage, G. A. Abers, and E. S. Cochran (2013). Potentially induced
566 earthquakes in Oklahoma, USA: Links between wastewater injection and the 2011 Mw 5.7
567 earthquake sequence, *Geology* 41, 699–702, doi: 10.1130/G34045.1.
568
569 Langenbruch, C., and M. D. Zoback (2016). How will induced seismicity in Oklahoma respond
570 to decreased saltwater injection rates?, *Sci. Adv.*, 2(11), e1601542, doi:10.1126/sciadv.1601542.
571
572 Lawson, J. E. and K. V. Luza (1995). Earthquake map of Oklahoma (with explanatory text),
573 *OGS Geologic Map* 35, Scale 1:500,000.
574
575 Luza, K. V. and J. E. Lawson (1982). Seismicity and tectonic relationships of the Nemaha uplift
576 in Oklahoma-Part IV, *OGS Special Publication* 82-1.
577
578 Luza, K. V., R. F. Madole, and A. J. Crone (1987). Investigation of the Meers fault,
579 southwestern Oklahoma, *OGS Special Publication* 87-1.
580
581 Marsh, S. and A. A. Holland (2016). Comprehensive Fault Database and Interpretive Fault Map
582 of Oklahoma, *OGS Open File Report* OF2-2016: 2 plates with supplement, 15 pages.
583
584 Murray, K.E., and Holland, A.A. (2014). Inventory of Class II Underground Injection Control
585 Volumes in the Midcontinent, *Shale Shaker*, v. 65, no. 2, p. 98-106.
586
587 OCC (2015). Oil and Gas Disposal Well Volume Reduction Plan,
588 http://www.occeweb.com/News/08-03-15VOLUME%20ADVISORY%20RELEASE.pdf
589 (Accessed August 2019).
590
591 OCC (2016a). Regional Earthquake Response Plan for
592 Central Oklahoma and Expansion of the Area of Interest,
593 http://www.occeweb.com/News/2016/03-07-16ADVISORY-
594 AOI,%20VOLUME%20REDUCTION.pdf (Accessed August 2019).
595

OCC (2016b). New Year, New Plays, New Plans, http://www.occeweb.com/News/2016/12-20-16SCOOP-STACK.pdf (Accessed August 2019).

Petersen, M.D. et al. (2014), Documentation for the 2014 update of the United States national seismic hazard maps: U.S. Geological Survey Open-File Report 2014–1091, 243 p., https://dx.doi.org/10.3133/ofr20141091.

Petersen, M. D. et al. (2016). 2016 One-Year Seismic Hazard Forecast for the Central and Eastern United States from Induced and Natural Earthquakes. Open-File Report, (June), 1–50. https://doi.org/10.3133/OFR20161035

Petersen, M. D. et al. (2017). 2017 One□Year Seismic□Hazard Forecast for the Central and Eastern United States from Induced and Natural Earthquakes. Seismological Research Letters, 88(3), 772–783. https://doi.org/10.1785/0220170005

Petersen, M. D. et al. (2018). 2018 One□Year Seismic□Hazard Forecast for the Central and Eastern United States from Induced and Natural Earthquakes. Seismological Research Letters. https://doi.org/10.1785/0220170005.

Pritchett, B. N., J. C. Chang, J. M. Chang, N. H. Suneson, and J. I. Walter (2017). Preliminary Soil Amplification Map of Oklahoma According to the National Earthquake Hazard Reduction Program (NEHRP), *OGS Geologic Map* 41, scale 1:500,000.

Regmi, N. and J. I. Walter (2019). Detailed Mapping of Shallow Landslides in Eastern Oklahoma and Potential Triggering by Oklahoma Earthquakes, *Geomorphology*, https://doi.org/10.1016/j.geomorph.2019.05.026.

Rosson, Z., J. I. Walter, T. Goebel, and X. Chen (2019). Narrow spatial aftershock zones for induced earthquake sequences in Oklahoma, *Geophys. Res. Lett.*, in review after revision.

Shah, A. K., and G. R. Keller (2017). Geologic influence on induced seismicity: Constraints from potential field data in Oklahoma, *Geophys. Res. Lett.*, 44, 152–161, doi:10.1002/2016GL071808.

Skoumal, R. J., R. Ries, M. R. Brudzinski, A. J. Barbour, and B. S. Currie (2018). Earthquakes induced by hydraulic fracturing are pervasive in Oklahoma, *J. Geophys. Res. Solid Earth*, 123. https://doi.org/10.1029/2018JB016790.

634 Skoumal, R. J., J. O. Kaven, and J. I. Walter (2019). Characterizing Seismogenic Fault Structures
635 in Oklahoma Using a Relocated Template□Matched Catalog, *Seismol. Res. Lett.*, doi:
636 https://doi.org/10.1785/0220190045.
637
638 Sumy, D. F., C. J. Neighbors, E. S. Cochran, and K. M. Keranen (2017). Low stress drops
639 observed for aftershocks of the 2011 Mw5.7 Prague, Oklahoma earthquake, *J. Geophys. Res.*
640 *Solid Earth*, 122, 3813-3834, doi:10.1002/2016JB013153.
641
642 Stocker, M., J. Baffes, Y. Some, D. Vorisek, and C. Wheeler (2018). "The 2014-16 Oil Price
643 Collapse in Retrospect: Sources and Implications." *Policy Research Working Paper 8419*, World
644 Bank, Washington, DC.
645
646 Walsh, R. R., and M. D. Zoback (2015). Oklahoma's recent earthquakes and saltwater disposal,
647 *Sci. Adv.* 1, e1500195, doi: 10.1126/sciadv.1500195.
648
649 Walter, J. I., J. C. Chang, and P. J. Dotray (2017). Foreshock seismicity suggests gradual
650 differential stress increase in the months prior to the 3 September 2016 Mw 5.8 Pawnee
651 earthquake, *Seismol. Res. Lett.*, 88(4), doi:10.1785/0220170007.
652
653 Walter, J. I., C. Frohlich, and T. Borgfeldt (2018). Natural and induced earthquakes in the Texas
654 and Oklahoma Panhandles, *Seismol. Res. Lett.*, 89 (6): 2437-2446,
655 https://doi.org/10.1785/0220180105.
656
657 Weber, B., Becker, J., Hanka, W., Heinloo, A., Hoffmann, M., Kraft, T., Pahlke, D., Reinhardt,
658 J., Saul, J., and Thoms, H. (2007). SeisComP3 – automatic and interactive real time data
659 processing, *Geophysical Research Abstracts*, vol. 9 of EGU General Assembly.
660
661 Weingarten, M., S. Ge, J. W. Godt, B. A. Bekins, and J. L. Rubinstein (2015). High-rate
662 injection is associated with the increase in U.S. mid-continent seismicity, *Science* 348, 1336–
663 1340.
664
665 Uhrhammer, R.A. and E.R. Collins (1990). Synthesis of Wood-Anderson seismograms from
666 broadband digital records, *Bull. Seism. Soc. Am.*, 80, 702-716.
667
668 Yeck, W. L., G. P. Hayes, D. E. McNamara, J. L. Rubinstein, W. D. Barnhart, P. S. Earle, and H.
669 M. Benz (2016). Oklahoma experiences largest earthquake during ongoing regional wastewater
670 injection hazard mitigation efforts, *Geophys. Res. Lett.* 43, doi: 10.1002/ 2016GL071685.
671
672 Yeck, W. L., M. Weingarten, H. M. Benz, D. E. McNamara, E. A. Bergman, R. B. Herrmann, J.
673 L. Rubinstein, and P. S. Earle (2016). Far-field pressurization likely caused one of the largest

injection induced earthquakes by reactivating a large preexisting basement fault structure, *Geophys. Res. Lett.* 43, 10,198–10,207, doi: 10.1002/ 2016GL070861.

Table 2

Station	Network	Latitude	Longitude	Elevation (m)	Sample Rate (Hz)	Datalogger	Sensor Type
AMES	OK	36.3357	-98.1930	394	100	RT130	Silicon Audio 203P
ARCA	O2	35.7430	-97.2695	323	100	RT130	Guralp CMG-3T Broadb
BLOK	OK	36.7607	-97.2150	301	100	RT130	Guralp CMG-6T
BLUF	OK	35.6567	-97.6093	302	100	RT130	Silicon Audio, 203P
CHAN	O2	35.6530	-96.7855	266	100	RT130	Streckeisen STS-2
CHOK	OK	35.5612	-97.0615	338	100	RT130	Guralp CMG-6T
CRES	O2	36.0372	-97.5345	311	100	RT130	Streckeisen STS-2
CROK	OK	36.5047	-97.9833	403	100	RT130	Guralp CMG-C3ESPC
CSTR	OK	35.6455	-98.6888	516	100	RT130	Guralp CMG-6T
DEOK	OK	35.8427	-96.4983	291	100	RT130	Guralp CMG-6T
DOVR	O2	35.9543	-97.9882	337	100	RT130	Guralp CMG-3T
DRUM	O2	35.9192	-96.6053	296	100	RT130	Streckeisen STS-2
ELIS	OK	36.0653	-99.4180	641	100	RT130	Guralp CMG-6T
FNO	OK	35.2572	-97.4007	357	100	RT130	Guralp CMG-C3ESPC
FRLY	OK	35.4153	-97.4513	387	100	RT130	Guralp CMG-6T
FW01	O2	36.4947	-98.9407	431	100	RT130	Guralp CMG-3T
FW02	O2	36.3783	-98.7293	462	100	RT130	Guralp CMG-3T
FW03	O2	36.5268	-99.1730	628	100	RT130	Guralp CMG-3T
FW04	O2	36.5960	-98.6652	449	100	RT130	Guralp CMG-3T
FW05	O2	36.4703	-98.6053	444	100	RT130	Guralp CMG-3T
FW06	O2	36.5138	-98.4990	420	100	RT130	Guralp CMG-3T
FW07	O2	36.4512	-98.8017	409	100	RT130	Guralp CMG-3T
FW08	O2	36.2383	-98.7967	559	100	RT130	Guralp CMG-3T
FW09	O2	36.5508	-99.0407	517	100	RT130	Guralp CMG-3T
FW10	Y9	36.5060	-98.7185	457	100	RT130	Guralp CMG-3T
GC02	OK	36.8515	-97.8597	354	100	RT130	OYO 2Hz MiniSeismom
GORE	O2	36.7847	-97.9415	348	100	RT130	Nanometrics Trillum
HTCH	OK	36.0170	-98.3327	347	100	RT130	Guralp CMG-6T
LOOK	OK	33.9925	-97.1800	287	100	RT130	Guralp CMG-6T
MOOR	OK	35.3418	-97.6592	371	100	RT130	Guralp CMG-6T
MRSH	O2	36.1323	-97.6955	309	100	RT130	Streckeisen STS-2
NOKA	OK	36.6347	-98.9320	476	100	RT130	Guralp CMG-6T
PERK	O2	35.9260	-97.1295	288	100	RT130	Streckeisen STS-2
PERY	O2	36.2600	-97.2350	209	100	RT130	Streckeisen STS-2
POCA	O2	35.2177	-98.0753	396	100	RT130	Streckeisen STS-2
PW01	Y7	36.4017	-96.9292	322	200	RT130	Sercel L-22 Short-Peric
PW02	Y7	36.4188	-96.8582	314	200	RT130	Sercel L-22 Short-Peric
PW03	Y7	36.4197	-96.8225	306	200	RT130	Sercel L-22 Short-Peric
PW05	O2	36.4850	-96.9640	289	200	RT130	Streckeisen STS-2
PW06	Y7	36.4207	-96.9720	303	200	RT130	Sercel L-22 Short-Peric
PW07	O2	36.5042	-96.7650	282	200	RT130	Streckeisen STS-2
PW08	O2	36.4058	-96.7328	275	100	RT130	Streckeisen STS-2
PW09	O2	36.4480	-96.8170	291	200	RT130	Streckeisen STS-2
PW10	O2	36.3655	-96.8310	297	200	RT130	Streckeisen STS-2
PW13	O2	36.3283	-96.8178	290	100	RT130	Streckeisen STS-2
PW15	O2	36.4685	-97.0137	270	200	RT130	Streckeisen STS-2